Biomed Microdevices (2012) 14:603–612
DOI 10.1007/s10544-012-9639-6

Porous polysulfone coatings for enhanced drug delivery

Kartik M. Sivaraman · Christoph Kellenberger · Salvador Pané · Olgaç Ergeneman · Tessa Lühmann · Norman A. Luechinger · Heike Hall · Wendelin J. Stark · Bradley J. Nelson

Published online: 4 March 2012

Abstract The synthesis of a porous polysulfone (PSU) coating for use in drug delivery applications is presented. PSU can serve as a functional surface coating for drug delivery vehicles, such as intraocular biomicrorobots. The coatings can be applied using spin coating or dip coating. The porosity is introduced by selectively dissolving calcium carbonate nanoparticles embedded in the bulk polymer. The network of pores thus formed increases by a factor of thirty the amount of Rhodamine B (model drug) that can be loaded and by a factor of fifteen the amount that can be released. The films do not affect cell viability and exhibit poor cell adhesion. The straightforward synthesis and predictability of porosity enables the tuning of the amount of drug that can be loaded.

Keywords Drug delivery · Porous membranes · Polysulfone · Microrobotics

1 Introduction

Drug delivery systems (DDS) are designed to enhance the efficacy of therapeutic agents by enabling their targeting and controlled release. An ideal DDS delivers medication exclusively to the diseased part of the body and releases it in a controlled manner. DDS have already enhanced the performance of many existing drugs and have resulted in the development of

Dedicated to the memory of Heike Hall who passed away in July 2011.

This work is supported by the NCCR Co-Me of the Swiss National Science Foundation and the CHIRP project of the ETH Zurich. Salvador Pané acknowledges the postdoctoral fellowship of Spanish MICINN.

K. M. Sivaraman (✉) · S. Pané · O. Ergeneman · B. J. Nelson
Multi Scale Robotics Lab,
Institute of Robotics and Intelligent Systems (IRIS),
ETH Zurich, Zurich 8092, Switzerland
e-mail: kartiks@ethz.ch

S. Pané
e-mail: vidalp@ethz.ch

O. Ergeneman
e-mail: oergeneman@ethz.ch

B. J. Nelson
e-mail: bnelson@ethz.ch

C. Kellenberger · N. A. Luechinger · W. J. Stark
Department of Chemistry and Applied Biosciences,
Functional Materials Laboratory,
ETH Zurich, Zurich 8093, Switzerland

C. Kellenberger
e-mail: christoph.kellenberger@chem.ethz.ch

N. A. Luechinger
e-mail: norman.luechinger@chem.ethz.ch

W. J. Stark
e-mail: wendelin.stark@chem.ethz.ch

T. Lühmann · H. Hall
Department of Materials, Cell and BioMaterials,
ETH Zurich, Zurich 8093, Switzerland

T. Lühmann
e-mail: tessa.luehmann@mat.ethz.ch

Present Address:
T. Lühmann
Department of Pharmacy and Food Chemistry, University of Würzburg, Am Hubland, 97074 Würzburg, Germany
e-mail: t.luehmann@pharmazie.uni-wuerzburg.de

completely new therapies as well (LaVan et al. 2003). In recent years, they have been miniaturized to the micro/nanoscale with the aim of improving the pharmacokinetics, biodistribution, and solubility of drugs (Allen and Cullis 2004). These efforts in scaling down have created various challenges. For example, the devices must be able to accommodate a clinically relevant amount of drug, must comply with biocompatibility and non-toxicity standards, and methods must be developed to measure their performance. Drug delivery has now become a multidisciplinary science where chemistry, microfabrication, nanotechnology, biology, and medicine all converge. Broadly, DDS that use nanostructured or nanoscale materials can be divided into two categories (LaVan et al. 2003; Allen and Cullis 2004).

- Therapeutic agents bound to nanoscale platforms such as nanoparticles, liposomes or micelles that can be introduced parenterally.
- Implants with nanoporous materials that act as reservoirs releasing the drug in a sustained manner.

Nanoparticles are especially suitable for DDS applications because of their large surface-area-to-volume ratio that helps in binding a large amount of drug (De Jong and Borm 2008). The nanoparticle platform can be made of inorganic substances such as gold (Paciotti et al. 2004), iron (Gupta and Gupta 2005), and silica (Liong et al. 2008). Apart from the therapeutic agents, other molecules or chemical ligands are also attached to these particles. They help in targeting specific tissues, improve the imaging of these particles and help the particles stay in circulation for a longer time inside the body. Nanoparticle-based DDS made of liposomes and biodegradable polymers are gaining more attention because of their efficiency in penetrating the fenestrated endothelium of tumors due to the enhanced permeability and retention effect (EPR, Peer et al. 2007). Once they gain access to tumors, they persist and release their contents and raise local drug concentrations inside the tumors. However, despite the vast amount of scientific literature available, there are lingering concerns about the toxicity of nanoparticle-based DDS. Due to the novel nature and extremely small size (ranging between 1 and 100 nm) of these materials, their long term effects on the body are not yet well understood, thus restricting their commercial use (Lewinski et al. 2008).

Advances in MEMS fabrication technology has already resulted in the commercialization of lab-on-a-chip devices for medical diagnosis and pushed forward the development of scaffolds for tissue engineering, stents, and implantable drug delivery devices (Tao and Desai 2002). These implants may release the encapsulated drug either due to changes in the implants' surroundings or due to external triggers like magnetic fields, light, or ultrasound (Sershen and West 2002). Most of these systems demonstrate the use of polymers and their interesting porous properties at the micro/nanoscales. Due to their high surface-area-to-volume ratio, nanoporous polymers show increased adsorption of molecules and, therefore, can be used in drug loading and release. In Yan et al. (2009), nanoporous polymer membranes have proven to increase the release of the model drug Rhodamine B by a factor of two compared to their nonporous counterparts .

The use of a wirelessly guided microrobot has been proposed for performing robotic surgery and for targeted drug delivery (Nelson et al. 2010). Although intended primarily for intraocular applications, the microrobot is envisaged for use in other parts of the human body as well. It is made of magnetic materials that are patterned using standard MEMS fabrication techniques and can be precisely maneuvered in three-dimensional space using a custom designed system of electromagnets (Kummer et al. 2010). A wireless intraocular oxygen sensor concept has been demonstrated using this microrobot (Ergeneman et al. 2010). For drug delivery applications, the surface area of the microrobot has been identified as the factor limiting the amount of drug that can be adsorbed or immobilized onto it (Ergeneman et al. 2008). Implementing a porous functional coating on the microrobot can increase its drug loading capacity by increasing the surface area of the device. For a fixed macroscopic volume of a functional polymer coating, those which are porous demonstrate an enhanced ability to adsorb and release Rh-B than planar coatings of the same polymer (Sivaraman et al. 2010).

In this work, we present the development of a porous coating made of polysulfone (PSU) that is envisaged for use in targeted drug delivery applications using the microrobot. PSU is a high performance biocompatible polymer (Wenz et al. 1990) which is already in use in medical equipment such as blood dialysis membranes (Gastaldello et al. 2001). The application of PSU capillary fibers for intraocular drug delivery has been reported (Rahimy et al. 1994). To produce the coating, a suspension of calcium carbonate ($CaCO_3$) nanoparticles in PSU was coated onto a substrate and the nanoparticles were selectively removed resulting in a network of nanometer-sized pores in the PSU. Such a protocol has been successfully used in Luechinger et al. (2010) to produce nanoporous membranes of silver. Apart from the enhanced drug adsorption and release of Rh-B from these porous PSU coatings, the

viability and adhesion of cells on these coatings are also investigated in this work.

2 Materials and methods

2.1 Synthesis of the $CaCO_3$ nanoparticles by flame spray pyrolysis

The $CaCO_3$ nanoparticles were synthesized using the flame spray pyrolysis (FSP) technique. Although a relatively new technique, FSP can produce nanoparticles with a wide and complex range of chemical compositions. In the FSP method, a liquid precursor in the form of fine droplets is fed to a flame in a reactor. This causes a reaction between the components of the precursor, thus, producing nanoparticles. The chemical composition of the precursor and the composition and flow of the fuel mixture producing the flame are important parameters in the FSP process (Maedler et al. 2002; Stark and Pratsinis 2002).

The $CaCO_3$ nanoparticles were synthesized by adopting the protocol given in Huber et al. (2005). A precursor consisting of 9 wt% calcium hydroxide ($Ca(OH)_2$, 99.9%, Aldrich) dissolved in equivalent volumes of 2-ethylhexanoic acid ($CH_3(CH_2)_3CH(C_2H_5)CO_2H$, ≥95%, Fluka) and xylene ($C_6H_4(CH_3)_2$, 96%, Riedel de Haen). The precursor was fed to a methane/oxygen (CH_4/O_2) flame sustained by feeding methane and oxygen at inlet rates of 9 ml.min^{-1} and 9 l.min^{-1}, respectively. To collect the nanoparticles, a glass fiber filter (Whatmann Ltd., USA) was mounted in the reactor above the flame. The off gas containing the nanoparticles was passed through the filter using a vacuum pump (Busch S.A., Switzerland).

2.2 Characterization of $CaCO_3$ nanoparticles

The diameters of the particles were in a range of 20–50 nm (Fig. 1, Philips CM 12, Philips CM 12, Philips, the Netherlands). X-ray diffraction (XRD) measurements performed using Cu Kα radiation (X'Pert Pro MPD, Pananalytical, The Netherlands) confirmed the crystalline nature of the particles. Thermo-gravimetric Analysis (TGA) experiments (Fig. 2) using 32 mg of the powder resulted in a change in mass of 35%. Upon heating, calcium carbonate decomposes to yield calcium oxide (CaO) and carbon dioxide (CO_2) gas as shown in Eq. 1. It was determined that the particles consisted of 20 wt% of calcium oxide (CaO) and 80 wt% $CaCO_3$.

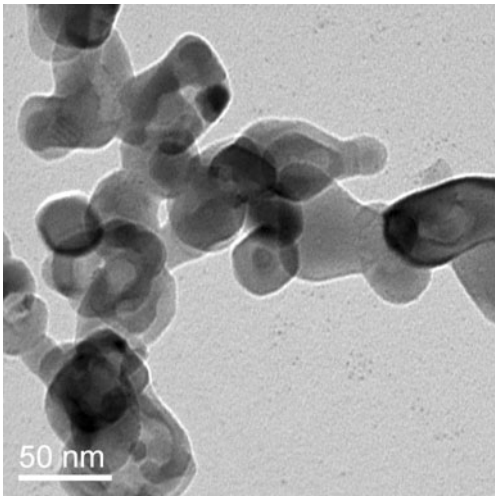

Fig. 1 Transmission electron micrograph of the flame synthesized $CaCO_3$ nanoparticles. The acceleration voltage used was 100 kV. The diameter of the particles was between 20 nm and 50 nm

$$CaCO_{3(s)} \rightarrow CaO_{(s)} + CO_{2(g)} \quad (1)$$

2.3 Preparation of the PSU-$CaCO_3$ composite films

A 15 wt% solution of PSU (Udel P-1700, Dolder AG, Switzerland) in dichloromethane (CH_2Cl_2, J.T. Baker) was prepared by stirring the components for 12 h at room temperature. $CaCO_3$ nanoparticles were added to the PSU while maintaining the following ratios by weight:

- $CaCO_3 : PSU = 1 : 1.105$
- $CaCO_3 + PSU : CH_2Cl_2 = 1 : 17.5$

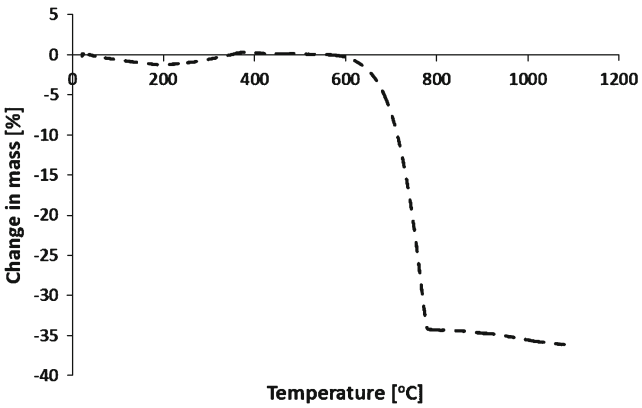

Fig. 2 The thermogram of the $CaCO_3$ nanoparticle powder. A change in mass of 35% was observed when 32 mg of the powder was used for the analysis

The $CaCO_3$: PSU ratio was maintained guided by the realization that too few particles would result in them being too far apart in the polymer to form an interconnected matrix, while a high concentration of these particles would cause the coating to collapse once these particles were dissolved. The $CaCO_3$ + PSU : CH_2Cl_2 ratio was important to ensure a suitable viscosity of the particle-polymer mixture. The viscosity and the coating parameters eventually determined the thickness of the composite film. The particle-polymer mixture was mixed in a vortexer and sonicated (1 min @ 240 W and 24 kHz) to obtain a suspension that remained stable for 12 h.

To synthesize the composite film, 500 μl of the particle-polymer mixture was pipetted onto a square silicon chip with an area of 2.25 cm^2 and spin-coated for 1 min at a speed of 1000 rpm and an acceleration of 1000 $rpm.s^{-1}$. The chip was then dried in air for 1 min and immersed in a 1% HCl solution for 5 min to dissolve the $CaCO_3$ particles. The bulk PSU films were also prepared using these spin coating parameters (Fig. 3). The morphology of the porous as well as bulk PSU coatings were observed by SEM (Zeiss Leo 1530 Gemini, Carl Zeiss AG, Germany).

2.4 Rhodamine B loading and release

Rhodamine B (Rh-B) is a fluorescent molecule roughly 1.6 nm in size and has been widely used as a model drug to study the behavior of novel drug delivery systems (Oh et al. 2008; Yan et al. 2009). Although it has little clinical significance, the convenience of detecting it through fluorescence spectrometry makes it a suitable molecule to evaluate the drug loading performance of porous coatings. For loading Rh-B, each coated chip was immersed in a well plate containing 2 ml of the dye solution (2 $g.l^{-1}$ of Rh-B in phosphate buffered saline (PBS), both from Sigma) per well for 18 h at room temperature in a dark environment. The loosely attached dye molecules were removed by washing the chips three times with Millipore-Milli-Q water, each cleaning step lasting 15 s.

The chips were then transferred into a new well plate containing 750 μl of PBS solution per well and stored in a dark environment. At the point of time of measuring the amount of Rh-B released, the chips were removed and transferred into a new well plate containing 750 μl of PBS per well and stored in the dark. From the PBS containing the released dye, 200 μl was pipetted out into a 96-well microplate reader. This procedure was repeated at 10 min intervals in the first half hour and later at 30 min intervals until 4 h. The fluorescence of the released Rh-B was measured by a spectrophotometer (Tecan Infinite 200s, Tecan GmbH, Germany). An excitation wavelength of 540 nm and emission wavelength of 625 nm were used during the fluorescence measurements. The experiments were repeated over 10 samples for each of the porous PSU and the bulk PSU.

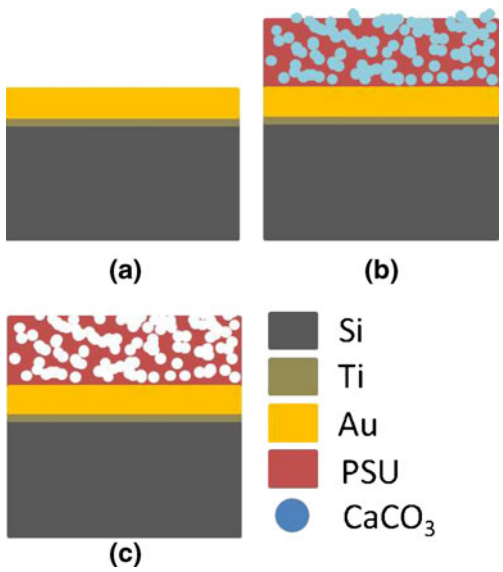

Fig. 3 Schematic of the preparation of porous PSU films. (**a**) The gold substrate obtained by e-beam evaporation on silicon. (**b**) The PSU-$CaCO_3$ composite film obtained by dip coating or spin coating. (**c**) The porous PSU film after the selective dissolution of $CaCO_3$ nanoparticles using HCl

2.5 Estimation of amount of Rhodamine B loading

To determine the amount of Rh-B loaded, the samples were prepared in exactly the same manner as in the release experiments: i.e. they were immersed in 2 ml of the dye solution (2 $g.l^{-1}$ of Rh-B in PBS) for 18 h at room temperature in a dark environment. The loosely attached dye molecules were removed by washing the samples three times with Millipore-Milli-Q water, each cleaning step lasting 15 s. The washed samples were placed in dark glass vials containing 2 ml of acetone (CH_3-CO-CH_3, reagent grade, Sigma) and left undisturbed for 48 h. Acetone was chosen as the medium for release because Rh-B is known to be more soluble in acetone than in aqueous media. The acetone containing the Rh-B was then transferred from the vials to a round bottom flask. To ensure the complete release of Rh-B from the membranes, they were further cleaned three times with acetone. Each time, 2 ml of acetone was pipetted into the vials, left standing for 2–3 min and transferred to the round bottom flask. The acetone in

the flask was vaporized in a rotatory evaporator to leave behind solid Rh-B. This was redissolved in water with a few drops of methanol (CH_3-OH, reagent grade, Sigma) being added to ensure complete dissolution. The solutions were analyzed using UV spectroscopy (Specord 200, Analytik Jena AG, Germany). The spectrum was scanned between 450 nm and 750 nm and an absorption peak was observed around 554 nm.

2.6 Fabrication of microrobot parts

The microrobot parts were fabricated using standard MEMS photolithography processes and electrodeposition. A titanium (Ti) adhesion layer of 50 nm and a copper (Cu) sacrificial layer of 500 nm were deposited on clean 4 inch silicon wafers using e-beam evaporation (E306A coating system, Edwards, UK). The wafers were subsequently patterned using a negative photoresist to produce moulds into which nickel (Ni) was electrodeposited. A table-top electrodeposition system (Iko Fibrotools Inc., USA) was used to deposit a 50 μm thick layer of Ni at a rate of approximately 1 $\mu m.min^{-1}$. Following the electrodeposition, the photoresist was stripped and the Ni microrobot parts were released by etching the underlying Cu.

Ni is known to be allergenic and sometimes also carcinogenic to humans (Kasprzak et al. 2003). Gold (Au) coatings show good biocompatibility and are widely used in dentistry and implants (Zitter and Plent 1987). In its final form, the microrobot is envisaged to have a a thin coating of Au in order to ensure that the bottom layer of the porous functional coating does not open directly onto Ni. Hence, Ni microrobot parts were coated with a 250 nm thick layer of Au using an electroless gold plating bath (Transene Company Inc., USA). Some of these gold-coated Ni parts were coated with the porous PSU using dip coating. The pieces were dipped into the particle-polymer suspension for 5 min and then dried in air for 1 min before being immersed in 1% HCl to remove the particles.

2.7 Biocompatibility tests

The gold coated Ni (Ni-Au) and the porous PSU dip-coated on gold coated Ni (Ni-Au-PSU) were used in biocompatibility experiments. Biocompatibility of the porous PSU coating was established by determining the viability and adhesion of normal human foreskin fibroblast (NHDF) cells on the coatings.

Cell viability tests Cell viability was determined by the water soluble tetrazolium (WST-1) proliferation and cytotoxicity test. The WST-1 essay has been used to determine the *in-vitro* biocompatibility of degradable biopolymers in cell cultures obtained from various ocular tissues (Huhtala et al. 1998). Upon reaction with various mitochondrial dehydrogenase enzymes, the light red colored tetrazolium salt is cleaved to yield a dark red water soluble dye called formazan which can be detected using a microplate reader. Therefore, the greater the amount of formazan detected, the greater the number of viable and metabolically active cells.

Proliferating NHDF (PromoCell, Germany) were harvested from exponentially growing subconfluent monolayers. The culture was maintained in 25 cm^2 culture flasks in Dulbecco's modified eagle medium (DMEM, GibcoBRL, Canada) supplemented with 10% heat inactivated fetal bovine serum (FBS, Sigma) and 1% antibiotic antimycotic (ABAM, GibcoBRL, Canada) at 37 °C and 5% CO_2. Cells were used until passage 20. A 2 $mg.ml^{-1}$ fibrin gel was used to sustain the NHDF during the course of the biocompatibility experiments. Human fibrinogen (Fluka) was mixed with 125 mM $CaCl_2$, then 2 $U.ml^{-1}$ of human thrombin (Sigma) was added as a catalyst to promote cross-linking of the gel. The gel was then transferred into a 96-well plate and the microrobot samples were incubated in this gel along with 3000 NHDF per sample. Prior to the transfer into the well plate, the Ni, Ni-Au and Ni-Au-PSU samples were sterilized for 20 min under UV light and stored in 0.1 M PBS solution at pH 7.4. As controls, 3000 NHDF were incubated with tissue culture polystyrene (TCPS) and unmodified fibrin gels under the same conditions. Mitochondrial activity was measured 24 h after seeding by the addition of 20 μl WST-1 solution (Roche) per sample and analyzing the absorption spectrum using a microplate reader (Infinite M200, Tecan GmbH, Germany).

Cell adhesion tests In order to visualize cell adhesion and cell viability of the NHDF on the surfaces of the microrobot samples, a live and dead staining was performed using the fluorescent stains fluorescein diacetate (FDA, Fluka) and Hoechst 33342 (Invitrogen). Living cells metabolize FDA to fluorescein and Hoechst 33342 intercalates itself with the DNA present in the nuclei of cells. On individual microrobots, 3000 NHDF were cultured for 48 h and stained with FDA (1 $mg.ml^{-1}$, 1:1000) and Hoechst 33342 in a PBS solution for 10 min at room temperature. A FITC filter and a DAPI filter were used to visualize fluorescein and Hoechst 33342 respectively under a fluorescence microscope (Zeiss Axiovert 200M, Carl Zeiss AG, Germany).

3 Results and discussions

3.1 Morphology

Figure 4(a) shows the cross section of bulk PSU films. It can be seen that the film is smooth and does not exhibit any porosity. Comparing the cross section of bulk PSU (Fig. 4(a)) with the surface (Fig. 4(b) and (c)) and the cross section of porous PSU (Fig. 4(d)), it becomes clear that porosity is not an inherent property of PSU, but occurs as a consequence of the dissolution of the embedded $CaCO_3$ nanoparticles. It is also observed that dip-coated films have fewer openings on their surface than spin-coated films. Spin coating enhances the rate of evaporation of the CH_2Cl_2 solvent, which rapidly increases the viscosity of the polymer-particle mixture. This results in the entrapment of a large amount of nanoparticles on the surface before they have the chance to sediment, thus creating more openings on the surface. Also, due to the rotational forces of the spin coating process, the polymer chains harden in a centro-symmetric manner, which could explain the wavy surface of the spin-coated samples (Yang et al. 1999, Fig. 4(c)).

3.2 Porosity

The chemistry behind the dissolution of the nanoparticles is shown in Eqs. 2 and 3.

$$CaCO_{3(s)} + 2HCl_{(aq)} \rightarrow CaCl_{2(aq)} + CO_{2(g)} + H_2O_{(l)} \quad (2)$$

$$CaO_{(s)} + 2HCl_{(aq)} \rightarrow CaCl_{2(aq)} + H_2O_{(l)} \quad (3)$$

Assuming that HCl dissolves all the embedded nanoparticles, the theoretically calculated porosity (ϕ_{th}) is:

$$\phi_{th} = \frac{v_{particles}}{v_{total}} \quad (4)$$

where $v_{particles}$ and v_{total} are the volume of the particles and volume of the particle-PSU composite, respectively.

Since the particle mass is a mixture of $CaCO_3$ (80%) and CaO (20%),

$$v_{particles} = \frac{m_{particles}}{\rho_{CaCO_3}} \times 0.8 + \frac{m_{particles}}{\rho_{CaO}} \times 0.2 \quad (5)$$

where $m_{particles}$ is the mass of particles in the composite, and ρ_{CaCO_3} and ρ_{CaO} are the densities of $CaCO_3$ and CaO particles, respectively. Assuming that the volumes are additive, the volume of the composite, v_{total}, is

$$v_{total} = \frac{m_{PSU}}{\rho_{PSU}} + v_{particles} \quad (6)$$

where m_{PSU} and ρ_{PSU} are the mass of PSU in the composite and the density of PSU, respectively.

Based on the ratios and substrate areas mentioned in Section 2.3, $m_{PSU} = 0.105$ g and $m_{particles} = 0.095$ g. Using the values, $\rho_{CaCO_3} = 2.73$ g.cm^{-3}, $\rho_{CaO} = 3.37$ g.cm^{-3}, $\rho_{PSU} = 1.24$ g.cm^{-3}, ϕ_{th} is 28.34%. The porosity was verified experimentally using the Brunauer–Emmett–Teller (BET) gas adsorption method (Micrometrics GmbH, Germany). The

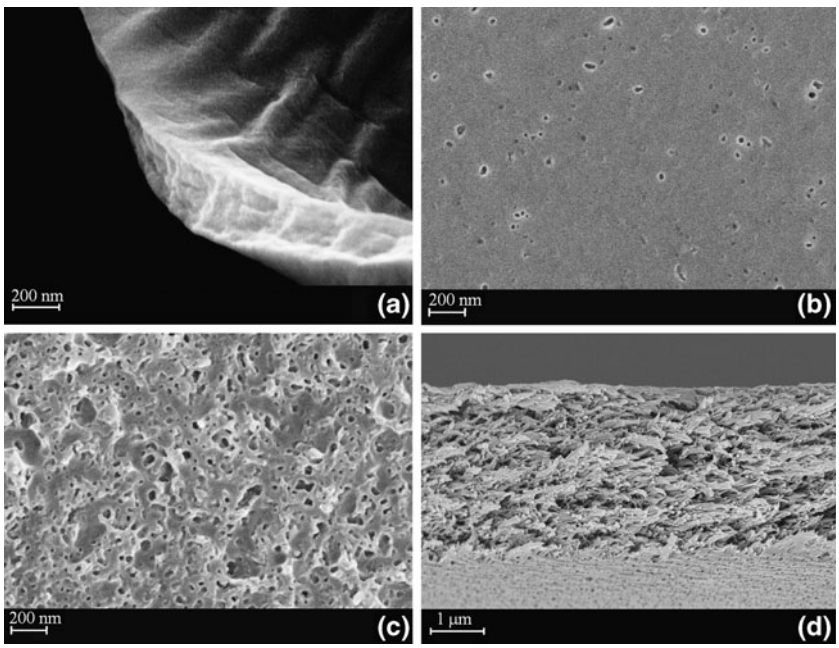

Fig. 4 SEM of bulk and porous PSU. (**a**) Cross section of bulk PSU films. (**b**) Surface of dip-coated porous PSU film. (**c**) Surface of spin-coated porous PSU film. (**d**) Cross section of spin-coated porous PSU film. The cross section was typical of both dip-coated and spin-coated PSU films

adsorbate used was nitrogen (N_2) at a temperature of 78K (Fig. 5). The measured porosity was 27.8%, which corroborates the assumption that all the embedded nanoparticles are dissolved by HCl. The ability to accurately predict the porosity would be pertinent to tune the amount of drug that can be loaded on a given volume of the polymer coating. The average diameter of the pores as determined by the BET measurements was around 26 nm which illustrates the nanoporous nature of the coating and is in good agreement with the TEM observations (Fig. 1).

3.3 Rhodamine B loading and release

In order to ensure a uniform coating thickness across all samples, the drug loading and release experiments were performed only on samples obtained by spin coating. The thickness of both bulk PSU and porous PSU coatings obtained was approximately 5 μm. The cumulative release of Rh-B from PSU coatings and bulk PSU is shown in Fig. 6. The amount of dye released is normalized over the macroscopic area of the substrate (2.25 cm^2). This was done because the projected area of a given thickness of both bulk PSU and porous PSU on the microrobot is the surface area of the microrobot. Hence, ultimately, the factor constraining the overall volume of a functional coating for our application is the macroscopic surface area of the microrobot. The porous PSU coatings show a fifteen-fold increase in the amount of Rh-B released compared to their bulk counterparts. The difference between the release behavior of the porous and bulk PSU indicated that the presence of pores was a key factor in encapsulation and release of Rh-B. While the release amount remains constant for the bulk PSU after the initial 20 to 30 min, the release from the porous PSU does not stabilize for almost 4 h. This suggests that the Rh-B is not confined to the outer surface of the porous PSU but percolates through its network of inter-connected pores, i.e. it is absorbed instead of just being adsorbed.

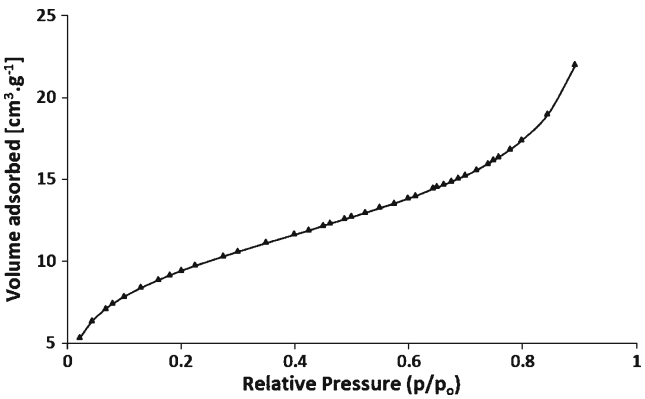

Fig. 5 The BET adsorption isotherm for porous PSU membranes. Nitrogen gas (N_2) at a temperature of 78 K was used as the adsorbate. The measured values of porosity and average pore size were 27.8% and 26 nm, respectively

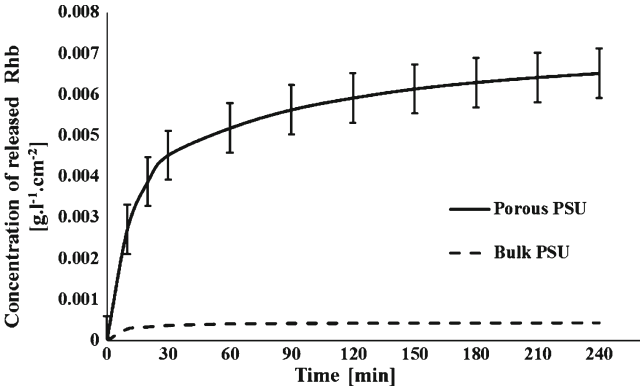

Fig. 6 Cumulative release graphs showing the average value of released Rhodamine B from porous PSU and bulk PSU. The *error bars* represent standard error of 10 samples over 2 separate sets of experiments

Table 1 compares the amount of Rh-B released after four hours with the estimated amount of dye loaded onto these membranes. While a significant portion of the estimated loaded amount of dye is released from the bulk membranes, only 36% of the amount of dye loaded onto porous membranes is released. This further corroborates the hypothesis that inter-connected pores of the porous membrane results in absorption, and, consequently to higher loading of the dye.

A common trait in both the porous and bulk PSU was that a significant amount of dye is released in the initial 20 min. This can be characterized as a burst release. Such a release was expected since it was solely dependent on diffusion. For intraocular drug delivery, a sustained drug release is required over a period lasting days to weeks. Such a release profile is usually obtained by suitably engineering the implant size, implant material, and the drug used (Bourges et al. 2006). However,

Table 1 Comparison between the amount of Rhodamine B loaded and the amount of dye released in PBS after 4 h from both bulk and porous samples

Membrane	Estimated loading		% Release
	Average	St. dev ($n = 5$)	
Bulk	0.5	0.16	80
Porous	16.5	0.7	36

The estimated amounts indicated are in $mg.l^{-1}.cm^{-2}$

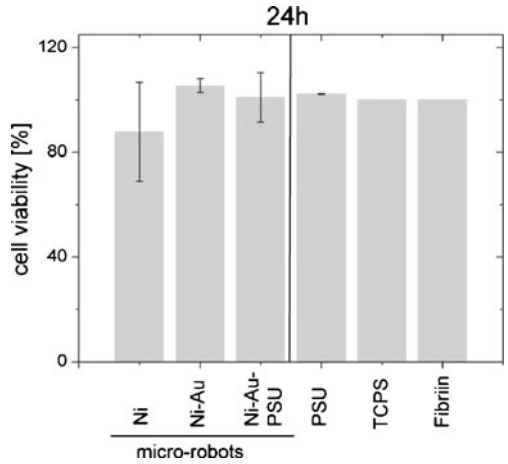

Fig. 7 Cell viability of NHDF incubated on various samples. The viability was determined by analyzing the mitochondrial activity of the NHDF using a WST-1 assay. The *error bars* represent mean values with standard deviation from three independent experiments carried out in triplicate

the amount of Rh-B loaded onto and released from the porous PSU compared favorably with the release rates of three drugs namely, 5-fluorouridine (5FUrd), triamcinolone (Triam), and human recombinant tissue plasminogen activator (t-PA) from the biodegradable ocular implants mentioned in Zhou et al. (1998). Since dip-coated PSU films obtained in the current work show fewer pores on their surface than spin-coated films, dip coating might be an option to suppress this tendency of burst release. This lack of pores on the surface, however, could lead to a decrease in the amount of drug that can be loaded onto the membrane. Another option to suppress the tendency of burst release might be adding a layer of bioerodible or biodegradable polymer onto the spin coated films. By tuning the rate of bioerosion/biodegradation of the layer, it might also be possible to obtain a sustained zero order release of therapeutic agents from the PSU membranes.

3.4 Cell viability tests

The viability of NHDF incubated for 24 h with Ni, Ni-Au and Ni-Au-PSU is shown in Fig. 7. Since the NHDF incubated with TCPS and unmodified fibrin gels were used as controls, the viability data from these controls were used to normalize the viability data from the other samples . Cell viability on the bulk PSU was nearly the same as on the controls, while that on bare Ni was the poorest. The viability on Ni-Au and Ni-Au-PSU was significantly better than on bare Ni.

3.5 Live and dead staining

The fluorescence microscope images of the live and dead staining performed on Ni, Ni-Au and Ni-Au-PSU (labeled as a, b, c respectively) are shown in Fig. 8. Green fluorescence from the FDA indicates living cells while blue fluorescence from Hoechst 33342 indicates cell nuclei. Despite the allergenic properties of Ni, the highest cell adhesion was detected on the Ni samples. The survival of cells on the Ni could be due to the lack of solvated Ni ions in the culture medium. The risk of cancer is said to be higher due to the reaction of Ni^{2+} ions with proteins and aminoacids rather than just the presence of elemental Ni in the body (Kasprzak et al. 2003). The International Committee on Nickel Carcinogenesis in Man suggested that less soluble forms of Ni pose a risk of cancer when present in concentrations above 10 $mg.m^{-3}$ in human beings (I.A. for Research on Cancer 1990).

The cell adhesion on the Ni-Au-PSU was the lowest. The low adhesion could be due to the hydrophobic nature of PSU. The hydrophobicity of bulk PSU is well established and is around 70° (Kim et al. 2002). Static contact angle measurements on the porous PSU yielded a value of $97° \pm 2°$. For applications involving drug release in the posterior segment of the eye, the lack of cell adhesion may actually work in favor of the porous PSU coating. Proliferation of retinal cells is the cause

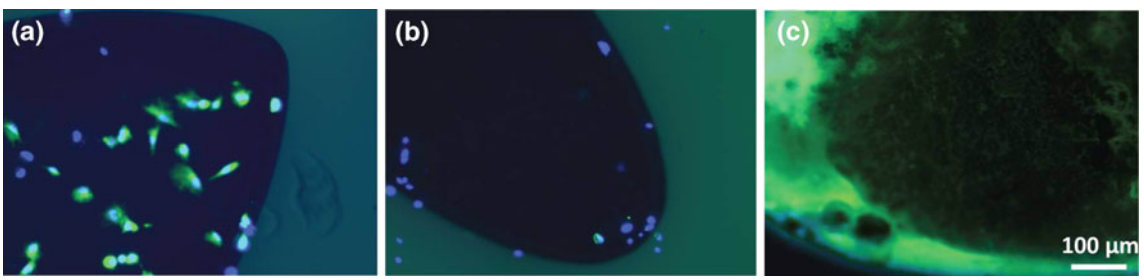

Fig. 8 Live and dead staining of NHDF on Ni (**a**), Ni-Au (**b**) and Ni-Au-PSU (**c**). *Green* fluorescence is from live cells while *blue* fluorescence is from cell nucleii. PSU coatings show a high degree of autofluorescence

for eye disorders such as proliferative vitreoretinopathy (PVR), and cell proliferation in general is the cause for many post-eye surgery complications (Colthurst et al. 2000). Also, the lack of cell adhesion would prevent clogging of the pores and, hence, lead to better predictability of the amount of drug released.

4 Conclusion

A porous, biocompatible, and non-toxic polymeric coating of polysulfone (PSU) was developed for drug delivery by selectively dissolving $CaCO_3$ nanoparticles embedded in bulk PSU coatings. The coating can be applied by dip or spin coating. The distinct difference in the morphology of bulk PSU and porous PSU confirms that the porosity is a result of the selective dissolving process. The porosity of the coatings as determined by BET measurements was 27.8% which closely matched theoretical predictions, thus demonstrating the relatively straightforward nature of synthesis. The suitability of the porous coating for enhanced drug loading and release was tested using Rhodamine B as a model drug. Although the porous coatings exhibited a burst drug release profile, they showed an enhanced adsorption and release which were on average 30 times and 15 times higher, respectively, compared to their nonporous counterparts of the same macroscopic volume. Cell viability tests with human foreskin fibroblast cells demonstrated that the viability of cells on the porous PSU is comparable to other commonly used biocompatible coatings such as gold. Also, cells showed a low level of adhesion on the porous PSU coatings, thus making the coating suitable for intraocular drug delivery.

References

T. Allen, P. Cullis, Drug delivery systems: entering the mainstream. Science **303**, 1818–1822 (2004)

J. Bourges, C. Bloquel, A. Thomas, F. Froussart, A. Bochot, F. Azan, et al., Intraocular implants for extended drug delivery: therapeutic applications. Adv. Drug Deliv. Rev. **58**, 1182–1202 (2006)

I.A. for Research on Cancer, in *Iarc Monographs on the Evaluation of Carcenogenic Risks to Humans*, vol 49, Chromium, Nickel and Welding (IARC Scientific Publications, 1990), pp. 257–445

M. Colthurst, R. Williams, P. Hiscott, I. Grierson, Biomaterials used in the posterior segment of the eye. Biomaterials **21**, 649–665 (2000)

W. De Jong, P. Borm, Drug delivery and nanoparticles: applications and hazards. Int. J. Nanomedicine **3**(2), 133–149 (2008)

O. Ergeneman, J.J. Abbott, G. Dogangil, B.J. Nelson, in *Functionalizing Intraocular Microrobots with Surface Coatings*. Proc. of 2008 Int. Conf. on Biomedical Robotics and Biomechatronics (BIOROB2008) (2008)

O. Ergeneman, G. Chatzipirpiridis, F. Gelderblom, J. Pokki, S. Pane, M. Toro, et al., in *Oxygen Sensing Using Microrobots*. Proc of the 32nd International Conference of the IEEE Engineering in Medicine and Biology Society (EMBC2010) (2010)

K. Gastaldello, C. Melot, R.J. Kahn, J.L. Vanherweghem, J.L. Vincent, C. Tielemans, Comparison of cellulose diacetate and polysulfone membranes in the outcome of acute renal failure. A prospective randomized study. Nephrol. Dial. Transplant. **15**(2), 224–230 (2001)

A. Gupta, M. Gupta, Synthesis and surface engineering of iron oxide nanoparticles for biomedical applications. Biomaterials **26**, 3995–4021 (2005)

M. Huber, W.J. Stark, S. Loher, M. Maciejewski, F. Krumeich, A. Baiker, Flame synthesis of calcium carbonate nanoparticles. Chem. Commun. (5), 648–650 (2005)

A. Huhtala, T. Pohjonen, L. Salminen, A. Salminen, K. Kaarniranta, H. Uusitalo, *In vitro* biocompatibility of degradable biopolymers in cell line cultures from various ocular tissues: extraction studies. J. Mater. Sci.-Mater. Med. **19**(2), 645–649 (1998)

K. Kasprzak, F. Sunderman, K. Salnikow, Nickel carcinogenesis. Mutat. Res. **533**(1–2), 67–97 (2003)

K. Kim, K. Lee, K. Cho, C. Park, Surface modification of polysulfone ultrafiltration membrane by oxygen plasma treatment. J. Membr. Sci. **199**, 135–145 (2002)

M. Kummer, J.J. Abbott, B.E. Kratochvil, R. Borer, A. Sengul, B.J. Nelson, Octomag: an electromagnetic system for 5-dof wireless micromanipulation. IEEE Trans. Rob. **26**(6), 1006–1017 (2010)

D.A. LaVan, T. McGuire, R. Langer, Small-scale systems for *in vivo* drug delivery. Nat. Biotechnol. **21**(10), 1184–1191 (2003)

N. Lewinski, V. Colvin, R. Drezek, Cytotoxicity of nanoparticles. Small **4**(1), 26–49 (2008)

M. Liong, J. Lu, M. Kovochich, T. Xia, S. Ruehm, A. Nel, et al., Multifunctional inorganic nanoparticles for imaging, targeting, and drug delivery. ACS Nano **2**(5), 889–896 (2008)

N. Luechinger, S. Walt, W.J. Stark, Printable nanoporous silver membranes. Chem. Mater. **22**, 4980–4986 (2010)

L. Maedler, H. Kammler, R. Mueller, S. Pratsinis, Controlled synthesis of nanostructured particles by flame spray pyrolysis. J. Aerosol Sci. **33**(2), 369–389 (2002)

B.J. Nelson, I.K. Kaliakatsos, J.J. Abbott, Microrobots for minimally invasive medicine. Annu. Rev. Biomed. Eng. **12**, 55–85 (2010)

J. Oh, R. Drumright, D. Siegwart, K. Matyjazewski, The development of microgels/nanogels for drug delivery applications. Prog. Polym. Sci. **33**(4), 448–477 (2008)

G. Paciotti, L. Myer, D. Weinreich, D. Goia, N. Pavel, McR. Laughlin, et al., Colloidal gold: a novel nanoparticle vector for tumor directed drug delivery. Drug Deliv. **11**(3), 169–183 (2004)

D. Peer, J. Karp, S. Hong, O. Farokhzad, R. Margalit, R. Langer, Nanocarriers as an emerging platform for cancer therapy. Nature Nanotechnology **2**, 751–760 (2007)

M.P. Rahimy, S. Chin, R. Golshani, C. Aras, H. Borhani, H. Thompson, Polysulfone capillary fiber for intraocular drug delivery: *In vitro* and *in vivo* evaluations. J. Drug Target. **2**, 2455–2480 (1994)

S. Sershen, J. West, Implantable, polymeric systems for modulated drug delivery. Adv. Drug Deliv. Rev. **54**, 1225–1235 (2002)

K.M. Sivaraman, K. Bayrakceken, O. Ergeneman, S. Pane, T. Luhmann, H. Hall, B.J. Nelson, in *Tailoring the Drug Loading Capacity of Polypyrrole Films for Use in Intraocular Biomicrorobots*. Proc. of the 32nd International Conference of the IEEE Engineering in Medicine and Biology Society (EMBC2010) (2010)

W.J. Stark, S. Pratsinis, Aerosol flame reactors for manufacture of nanoparticles. Powder Technol. **126**(2), 103–108 (2002)

S. Tao, T. Desai, Microfabricated drug delivery systems: from particles to pores. Adv. Drug Deliv. Rev. **55**, 315–328 (2002)

L. Wenz, K. Memitt, S. Brown, A. Moet, *In vitro* biocompatibility of polyetheretherketone and polysulfone composites. J. Biomed. Mater. Res. **24**, 207–215 (1990)

W. Yan, V. Hsiao, Y. Zheng, Y. Shariff, T. Gao, T. Huang, Towards nanoporous polymer thin film based drug-delivery systems. Thin Solid Films **517**(5), 1794–1798 (2009)

J.P. Yang, P.L. Heremans, R. Hoefnagels, W. Tachelet, P. Dieltiens, F. Blockhuys, H.J. Geise, G. Borghs, Blue organic light-emitting diode using 1,4-bis(1,1-diphenyl-2-ethenyl)benzene as emitter. Synth. Met. **108**(2000), 95–100 (1999)

T. Zhou, H. Lewis, R. Foster, S. Schwendeman, Development of a multiple-drug delivery implant for intraocular management of proliferative vitreoretinopathy. J. Control. Release **55**, 281–295 (1998)

H. Zitter, H. Plent, The electrochemical behavior of metallic implant materials as an indicator of their biocompatibility. J. Biomed. Mater. Res. **21**, 881–896 (1987)